Band Gap Tailoring, Size Modulation and Photoluminescence Properties of Mn/Cu doped ZnS Nanostructures

P.J. Binu

Government Arts College Melur Post Graduate & Research Department of Physics

S. Muthukumaran (drsmk123@yahoo.co.in)

H.H. The Rajah's College, Pudukkottai, Tamilnadu, India https://orcid.org/0000-0002-6050-0782

Research Article

Keywords: Mn, Cu dual doped ZnS, Tuning of size, Band gap tailoring, FTIR, Photoluminescence

Posted Date: February 12th, 2021

DOI: https://doi.org/10.21203/rs.3.rs-216184/v1

Abstract

ZnS, Mn added ZnS ($Zn_{0.97}Mn_{0.03}S$) and Mn, Cu dual doped ZnS ($Zn_{0.95}Mn_{0.03}Cu_{0.02}S$) QDs have been prepared using co-precipitation technique. The influence of Mn and Cu addition on the morphology, structure and photoluminescence properties of Mn/Cu incorporated ZnS have been examined. Cubic structure of the synthesized samples was confirmed by X-ray diffraction patterns. The incorporation of Cu in Zn-Mn-S lattice not only decreased the particle/grain size and also generates more defect based luminescent activation centres. The reduced energy gap by Mn addition was explained by sp-d exchange interaction and the elevated energy gap in Cu, Mn dual doped ZnS was expalined by Burstein–Moss effect. The tuning phenomenon of size as well as the energy gap in ZnS by Mn/Cu addition promote these materials for nano-electronic applications. FTIR spectra confirmed the presence of Mn/Cr-Zn-S bondings. The substitution of Mn /Cu provides an effective control over tuning of different emission colours which signifies their applications like light emitting diodes.

1. Introduction

ZnS is one of the most significant and extensively considered metal sulphides in the last several years due to its enhanced optical nature, broad energy gap and better luminescence behaviour at higher wavelength region [1, 2]. The two common structures of ZnS are wurtzite as well as zinc-blende and they have the band gap between 3.72 eV to 3.77 eV [3, 4]. The unique properties aroused from its size and structures leads them for diverse applications such as luminescence devices, photo-voltaics, ultraviolet LEDs, efficient solar cells and different lasers [5].

The addition of transition metal (TM) ions made an extraordinary variation in optical, structural, electrical and transition probabilities in the Zn-S lattice [6, 7]. Within the different TMs, Mn was chosen as the first doping material since it improves the emission properties, enhances the electrical, microstructural and optical characters and also possesses better photo and thermal stability [8]. Chandrasekar et al. [9] discussed the variation in Urbach energy, Stokes's shift and steepness values in Mn added ZnS synthesized by co-precipitation technique. Ashkarran et al. [10] revealed the decrease of photo-catalytic removal efficiency with the help of Bromocresol Green, Rhodamine B, and Bromochlorophenol Blue dyes in Mn added ZnS than un-doped ZnS. In order to avoid the impurity and secondary phase generation, Mn level is restricted as 3%.

It is noticed from the literature that the addition of Cu in ZnS induces the visible luminescence involving blue and green wavelengths whereas the addition of Mn fine-tune the emissions between blue and orange [11]. The simultaneous addition of Mn and Cu is useful to attain the dual emissions [12]. Moreover, the dual doping of Mn and Cu into ZnS enhanced its structural and optical properties by its unusual recombination patterns. Since the luminescence nature of ZnS is significantly modified by adjusting the small level of TM ions [13], the Mn and Cu addition into ZnS plays considerable role in the fine-tuning of emission properties in a well-controlled way.

The optical and structural evaluation of Mn or Cu doped ZnS [9–11] is available in the literature but the complete studies on Mn and Cu dual doped ZnS is nearly scanty. Therefore, Mn and Cu dual doped ZnS have been synthesized using co-precipitation method. In addition, the comprehensive structural and photoluminescence behaviour of Mn and Cu dual doped ZnS have been examined using the appropriate instruments. The deviation in size as a result of Mn/Cu doping was interconnected with the band gap of the materials. The effect of Mn as well as Cu on ZnS and the influence of defect sites in the photoluminescence properties have been discussed in detail.

2. Experimental Techniques

2.1. Preparation of ZnS, $Zn_{0.97}Mn_{0.03}S$ and $Zn_{0.95}Mn_{0.03}Cu_{0.02}S$

Zinc acetate ($Zn(CH_3COO)_2.2H_2O$, source of Zn^{2+}, anions) and sodium sulfide (Na_2S, source of S^{2-}, cations) have been taken as the precursors. Manganese acetate ($Mn(CH_3COO)_2.2H_2O$, source of Mn^{2+}, anions) and copper acetate ($Cu(CH_3COO)_2.4H_2O$, source of Cu^{2+}, anions) were selected as the dopant. Aqueous ammonia solution was used to change the pH of the solution. All the chemicals used in the present were in analytical grade (AR) with 99.99% purity purchased from M/s. Merck. Ultra pure de–ionized water was used as solvent throughout the synthesis process.

For the preparation of $Zn_{0.95}Cu_{0.02}Mn_{0.03}S$, 0.95M zinc acetate, 0.03 M manganese acetate 0.02M copper acetate were gradually dissolved (one by one) in 50 ml double distilled water and kept at constant stirring (at rate of 1000 rpm) at 80°C until a clear and homogeneous solution is obtained. Then, 50 ml 1 M sodium sulfide solution was added drop by drop to the above mixture solution under continuous stirring for 6 h. Aqueous ammonia solution was used to maintain the pH Value of the mixer solution as 9.5. After 6 h, a light gray to dark gray precipitate was deposited at the bottom of the flask. The wet precipitate was filtered out separately and washed with de-ionized water and methanol to remove unwanted impurities formed during the preparation process. Finally, obtained product was dried using micro-oven at 50–80° C for 5h. The final precipitates were grounded using an agate mortar. The flow chart for the preparation of Mn, Cu doped ZnS is as shown in Fig. 1.

For the preparation of pure ZnS, 1M zinc acetate alone used without manganese acetate and copper acetate. Similarly, for $Zn_{0.97}Mn_{0.03}S$ preparation, 0.97M zinc acetate and 0.03M manganese acetate were used without copper acetate. 0.95M zinc acetate, 0.03M manganese acetate and 0.02M copper acetate were used for the preparation of $Zn_{0.95}Mn_{0.03}Cu_{0.02}S$ nanostructures. The preparation procedure of the samples is same as discussed above.

2.2. Characterization techniques

The diffracted patterns were recorded by RigaKuC/max-2500 diffractometer using CuKa radiation (λ = 1.5406 Å) at 40 kV and 30 mA from 2θ = 20 to 70°. The UV–visible optical absorption and transmittance studies of ZnS, $Zn_{0.97}Mn_{0.03}S$ and $Zn_{0.95}Mn_{0.03}Cu_{0.02}S$ nanoparticles were carried out to investigate their optical properties using UV–visible spectrometer (Model: lambda 35, Make: Perkin Elmer) from 300 to 550 nm at ambient temperature. Halogen and deuterium lamps were used as sources for visible and UV radiations, respectively. The presence of chemical bonding was studied by Fourier transform infra-red (FTIR) spectrometer (Model: Perkin Elmer, Make: Spectrum RXI) from 400 to 4000 cm^{-1}. Pellets were prepared by mixing the nanoparticles with KBr at 1 wt%. Room-temperature photoluminescence (PL) behaviour have been taken out by a fluorescence spectrophotometer (Model: Hitachi, Make: F-2500) at excitation wavelength of 330 nm to study the emission properties of the materials.

3. Results And Discussion

3.1. XRD - Structural analysis

The XRD spectra of un-doped ZnS, Mn = 3% doped ZnS and Mn = 3% and Cu 2% dual doped ZnS QDs for the different diffraction angles (2θ) from 20° to 70° are presented in Fig. 2a. The noticed broad peaks indicate that the synthesized samples are in the nano-scale levels. The entire samples display the wide diffraction peaks about 28.5°, 48.7° and 57.5° and they are related to (111), (220), and (311) orientations, respectively. Here, the preferred orientation is along (111) plane due to its highest peak intensity throughout the entire samples. The attained three XRD peaks are matched well with the JCPDS card no: 80 – 0020 which reflected that all the synthesized samples posses the cubic structure of ZnS.

The XRD peak intensity of ZnS is decreased Mn doping and reduced further by Cu, Mn dual doping and the reduced peak intensity designates the size mutation and crystalline deterioration. Throughout this work, (111) orientation with higher XRD intensity is preferred to study the effect of doping (Mn/Cu) on ZnS. The current reduction in crystallinity reflects the disorder induced in the Zn-Mn-S lattice by the incorporation of Cu. The generation of extra or additional impurity / secondary phases such as Mn/Cu metals, Mn/Cu sulphides or Mn/Cu oxides are ruled out because no unwanted additional peaks were noticed in the XRD studies. Therefore, the present XRD patterns confirm the phase singularity without any extra phases of the prepared samples. No secondary or impurity phases found in the XRD analysis recommended that the doping elements Mn and Cu are appropriately substituted into Zn-S lattice [14]. The observed slight turn of XRD peaks along higher 2θ region by Cu addition also signifies that Cu is appropriately substituted into $Zn_{0.97}Mn_{0.03}S$ lattice. The identical shift along higher diffraction angles was reported in Ni added ZnS nanostrucutres by Kaur et al. [15]

Figure 2b shows the variation of FWHM and crystallite size of un-doped ZnS, $Zn_{0.97}Mn_{0.03}S$ and $Zn_{0.95}Mn_{0.03}Cu_{0.02}S$. The incorporation of Cu elevates the FWHM which reflects the shrinkage of crystallite size. The average crystallite size of the prepared nanostructures have been estimated with the help of Scherrer's formula [16], $0.9\lambda / \beta \cos\theta$, where β is FWHM in radian and θ is the diffraction angle.

Figure 2b clearly shows the slight increment in size by Mn doping and the significant reduction in size by Mn and Cu dual doping. The slight increase of size in Mn-doped ZnS is due to replacement of Mn^{2+} ions (ionic radius ~ 0.80 Å) in the position of Zn^{2+} (ionic radius ~ 0.74 Å) [17]. The same kind of size increment is noticed by Wang et al. [18] in Mn added ZnS.

The decrease of crystallite size at Cu addition is supported by the dissimilarity between the ionic radius between Cu and Zn. Here, the ionic radius of Cu^{2+} ions (≈0.71 Å) is smaller than the ionic radius of Zn^{2+} ions as well as Mn^{2+} ions. The decrease of size was discussed by Reddy et al. [19] at $Zn_{0.97-x}Cu_xCr_{0.03}S$ QDs with Cu > 3% and they described that the size reduction was due to the generation of lattice disorder by the Cu addition. Wang et al. [20] revealed that the simultaneous substitution of Mn^{2+} and Cu^{2+} ions were not homogeneously dispersed in Zn-S nanostructures but the core portion includes more Mn^{2+} ions and the surface portion contains much Cu^{2+} ions. It is concluded from the XRD analysis that the incorporation of Cu^{2+} ions weaken the size as well as produce the defect associated luminescence states.

3.2. Optical absorption and transmittance spectra

Optical absorption spectra of pure ZnS, Mn = 3% doped ZnS and Mn = 3% and Cu = 2% simultaneously doped ZnS within the wavelength ranging between 300 nm and 550 nm are illustrated in Fig. 3a. The absorption edge of all the three samples is well below the visible wavelength i.e., below 400 nm (~ 320 nm to 400 nm) [21]. Both the increase of absorption intensity as well as shift of absorption edge along long wavelength region are noticed by the substitution of Mn into Zn-S lattice ($Zn_{0.97}Mn_{0.03}S$). The elevated absorption intensity by Mn addition may be due to the increase of size and also the proper incorporation of Mn^{2+} ions in the position of Zn^{2+} ions where the ionic radius of Mn^{2+} ions is higher than Zn^{2+} ions. The modulation in crystallite size by Mn addition is the one more probable reasons for the noticed increment in absorption intensity and also the red shift of absorption edge. The same kind of red shift in absorption edge by Mn addition in ZnS was revealed by Li et al. [22]. One more literature [23] confirmed the shift of absorption edge along higher wavelength region by Mn addition in ZnO.

During the addition of Cu in Zn-Mn-S lattice, the absorption intensity suppressed to lower value and also the absorption edge moved along the lower wavelength region i.e., blue shift of energy gap. The existing blue shift of absorption edge was supported by the size reduction which promote the energy gap to higher value [24]. In addition, the Cu-doping stimulates more defect and creates the irregularity or imperfections through Zn-Mn-S lattice owing to the ionic radius variation among Cu^{2+}, Mn^{2+} and Zn^{2+} ions which may also the probable reason for the reduction in absorption intensity [25]. The light scattering by grain boundaries and the reflection of incident light by Cu clusters in $Zn_{0.95}Mn_{0.03}Cu_{0.02}S$ may also reduce the absorption intensity [19].

Figure 3b presents the transmittance spectra of pure ZnS, Mn = 3% doped ZnS and Mn = 3% and Cu = 2% simultaneously doped ZnS within the wavelength ranging between 300 nm and 550 nm. The whole samples reveal the semitransparent character with highest transmittance in the visible wavelength region. The observed rapid increase of transmittance along UV wavelength region throughout the samples is due

to the inter-band transition commencing from valence band level to conduction band. The percentage of transmittance in the visible region gets down by Mn-doping (single doping) and further diminished by double (Mn and Cu doping) doping where it varies between 50–75%.

3.3. Energy gap estimation

The inclusion of Mn and Cu into ZnS not only affect the absorption and transmittance and also tailored the energy gap of the synthesized samples. Therefore, to investigate the influence of Mn/ Cu through band structure as well as electronic transition, the correlation among the absorption coefficient and the photon energy was examined using Tauc's relation [26], $h\upsilon = A(h\upsilon - E_g)^n$, where, E_g is energy gap and the exponent 'n' is taken as 0.5. The linear part of 'hυ' designates the direct band gap of the samples.

The band gap of the synthesized materials is acquired from the plot between $(\alpha h\upsilon)^2$ and hυ as revealed in Fig. 4a. The band gap of pure ZnS is found to be 3.51 eV. The steep decrease in band gap from 3.51 eV (ZnS) to 3.28 eV ($Zn_{0.97}Mn_{0.03}S$, $\Delta E_g \sim 0.23$ eV) was noticed during the addition of Mn^{2+} in Zn-S lattice where Mn^{2+} may occupies either interstitial sites or substitutional positions of Zn^{2+} ions. The substitution of Mn^{2+} ions generates the dislocated or irregular atoms and induces the imperfections in the structural bonding of ZnS which are made by the 3d electrons in Mn atoms [21]. The stimulated sp-d exchange interaction by Mn between the s and p electrons from ZnS and 3d electrons from Mn^{2+} ions is responsible for the reduction in energy gap [27]. The addition of Mn re-generate the newer energy levels closer to the valence band of ZnS which is also the another possible reason for current shrinkage in energy gap [28].

The abrupt increase of energy gap from 3.28 eV ($Zn_{0.97}Mn_{0.03}S$) to 3.94 eV (($Zn_{0.95}Mn_{0.03}Cu_{0.02}S$, $\Delta E_g \sim$ 0.66 eV) was obtained by Cu doping where Cu^{2+} ions with lower ionic radius may be replace Zn^{2+} ions at substitutional sites. The addition of Cu liberates more free charge carriers in Zn-Mn-S lattice which modify the Fermi level and move closer to the conduction band and broadens the energy gap. The current enhancement in energy gap i.e., blue shift of energy gap by Cu doping is the Burstein-Moss shift [29]. The existence of poor crystallinity by Cu addition also play a major role in the increase of energy gap [30]. Figure 4b illustrates the change in average crystallite size and energy gap of un-doped ZnS, $Zn_{0.97}Mn_{0.03}S$ and $Zn_{0.95}Mn_{0.03}Cu_{0.02}O$ nanostructures. When Mn is introduced into ZnS energy gap reduced to lower value at the same time size of the nanoparticles enhanced slightly to higher value i.e., it obey the size effect [31]. Moreover Cu addition into Zn-Mn-S increases the energy gap which is in good agreement to the quantum confinement effect of the nanoparticles [32].

3.4. Fourier transform infrared (FTIR) studies

FTIR is the best technique to examine the chemical bonding in the substance and also to identify the organic group of the materials. The room temperature FTIR spectra of pure ZnS, $Zn_{0.97}Mn_{0.03}S$ and $Zn_{0.95}Mn_{0.03}Cu_{0.02}S$ are shown in Fig. 5 between 400 cm^{-1} and 4000 cm^{-1}. The wide absorption bands for all the samples within the range of 3000–3600 cm^{-1} related to OH stretching vibration which designates the survival of water absorbed in the surface of nanoparticles [33]. The observed bands

between 1592–1602 cm^{-1} ascribed to C = O stretching modes induced from the existing atmospheric CO_2 in the sample [34, 35]. The absorption bands centered at 1121 cm^{-1} are related to the partial substitution of Mn or Cu atoms into Zn position in Zn-S lattice [1]. The feeble and weak absorption band centered around 928 cm^{-1} corresponds to the defect states induced by Cu-substitution in Mn-Zn-S lattice which absent in other two samples. The strong bands about 670–676 cm^{-1} and 511–520 cm^{-1} are responsible for Zn-S stretching vibrations [36]. The bands corresponding to Zn-S show the better agreement with the earlier studies [37].

3.5. Photoluminescence (PL) spectra

In order to investigate the electronic inter-band transition and influence of doping on emission properties of pure ZnS, $Zn_{0.97}Mn_{0.03}S$ and Cu-doped $Zn_{0.97}Mn_{0.03}S$ samples, PL spectra have been recorded. Figure 6 shows the PL spectra of all the samples in the wavelength ranges from 350 nm to 650 nm at room temperature. Pure ZnS exhibits a wide and broad PL band within the wavelength range from 370 nm to 550 nm which is similar to the literature reported by Faita et al. [38]. The noticed wide emission band represents the existence of lower crystallite size (35 Å) where self activated defect states have been generated by different defects like oxygen defects, Zn interstitials, sulfur vacancies and point defects. Moreover, the presence of asymmetrical peak in ZnS proposes the involvement of many emission bands combined as broad peak with centre along violet and bluish-violet region [39].

Generally, the emission in the visible region arises from impurity or native defect levels. The intensity of the broad band corresponding to violet and bluish-violet emissions in ZnS is decreased sharply by Mn/Cu doping. During Mn-doping into ZnS, the violet emission shifted to higher wavelength side with reduced intensity. One of the reason to decrease the intensity and the red shift of wavelength is the increase of crystallite size which emits the longer wavelengths compared to lower size [40]. Nasser et al. reported that the reducing intensity by Mn addition is due to the diminishing rate of band to band recombination of charge carriers [41]. The observed diminishing emission intensity and the blue band emission at 486 nm by Cu-doping is due to the formation of luminescence centers that trap the electrons and holes and enhance the non-radiative recombination process [42].

Figure 7 shows the energy level diagram of the different synthesized samples to explain the various emissions like violet, blue and yellowish orange. In un-doped ZnS, the UV emission originated from band to band transitions and the other visible emissions induced by defect states related transitions [43]. When Mn is incorporated into ZnS, Mn^{2+} ions behaves as luminescence centers and make a strong inter-relation with s - p states of the host lattice [44]. Thus, Mn^{2+} substitution induces a strong characteristic emission along yellow to orange emission [15] as shown in Fig. 7. The strong and prominent band appeared at 587 nm (corresponding to orange emission) in Mn-doped ZnS (which is absent in ZnS) is associated with the electronic transition from $^4T_1$ to $^6A_1$ in the $3d^5$ intra-configurational of Mn^{2+} ions [45, 46]. The identical consequences have been described by Kole et al. [47] and Karar et al. [48] in Mn doped ZnS.

The elevated blue emission at 486 nm is the feature of Mn, Cu dual doping which arises from the transition of the electrons from the (surface states) conduction band of ZnS to the 't_2' levels of Cu impurities [48]. It is understood from Fig. 7 that the electrons are excited from ground state lower energy state to the conduction band and the electrons may relax to the defect states, from which they recombine through the d-orbital of Cu^{2+} ions or be transferred into the electronic levels of Mn^{2+} ions that guide to the characteristic Cu and Mn dopant emissions [20]. The acquired high intensity yellowish-orange emission in Mn/Cu-doped ZnS emphasizes their significance in the application of light emitting diodes and photonic applications.

4. Conclusions

Following are the conclusions drawn from the present investigations:

- ZnS, Mn added ZnS ($Zn_{0.97}Mn_{0.03}S$) and Mn, Cu dual doped ZnS ($Zn_{0.95}Mn_{0.03}Cu_{0.02}S$) QDs have been prepared using co-precipitation technique.
- The influence of Mn and Cu addition on the morphology, structure and photoluminescence properties of Mn/Cu incorporated ZnS have been examined.
- Cubic structure of the synthesized samples was confirmed by X-ray diffraction patterns.
- The incorporation of Cu in Zn-Mn-S lattice not only decreased the particle/grain size and also generates more defect based luminescent activation centres.
- The reduced energy gap by Mn addition was explained by sp-d exchange interaction and the elevated energy gap in Cu, Mn dual doped ZnS was expalined by Burstein–Moss effect.
- The tuning phenomenon of size as well as the energy gap in ZnS by Mn/Cu addition promote these materials for nano-electronic applications.
- FTIR spectra confirmed the presence of Mn/Cr-Zn-S bondings.
- The substitution of Mn /Cu provides an effective control over tuning of different emission colours which signifies their applications like light emitting diodes.

Declarations

Due to technical limitations, Declarations section is not available for this version.

References

1. Ummartyotin, N. Bunnak, J. Juntaro, M. Sain, H. Manuspiya, Synthesis and luminescence properties of ZnS and metal (Mn, Cu)-doped-ZnS ceramic powder, Solid State Sci. **14**, 299–304 (2012).
2. G. Alvarez-Coronadoa, L.A. Gonzáleza, J.C. Rendón-Ángelesa, M.A. Meléndez-Lirab, R. Ramírez-Bon, Study of the structure and optical properties of Cu and Mn in situ doped ZnS films by chemical bath deposition, Mat. Sci. Semicon. Proc. **81**, 68-74 (2018).

3. Göde, C. Gümüş, M. Zor, Investigations on the physical properties of the polycrystalline ZnS thin films deposited by the chemical bath deposition method, J. Cryst. Growth **299**, 136-141 (2007).
4. Haddad, A. Chelouche, D. Talantikite, H. Merzouk, F. Boudjouan, D. Djouadi, Effects of deposition time in chemically deposited ZnS films in acidic solution, Thin Solid Films **589**, 451-456 (2015).
5. Wang, H. Huang, B. Liang, Z. Liu, D. Chen, G. Shen, ZnS nanostructures: synthesis, properties, and applications, Crit. Rev. Solid State Mater. Sci. **38**, 57-90 (2013).
6. Cao, D. Han, B. Wang, L. Fan, H. Fu, M. Wei, B. Feng, X. Liu, J. Yang, Low temperature synthesis, photoluminescence, magnetic properties of the transition metal doped wurtzite ZnS nanowires, J. Solid State Chem. **200**, 317–322 (2013).
7. Viswanath, H.B. Naik, G.Y. Kumar, P.P. Kumar, G.A. Kumar, R. Praveen, EDTAassisted hydrothermal synthesis, characterization and photoluminescent properties of Mn^{2+}-doped ZnS, J. Lumin. **153**, 446–452 (2014).
8. Labiadh, B. Sellami, A. Khazri, W. Saidani, S. Khemais, Optical properties and toxicity of undoped and Mn-doped ZnS semiconductor nanoparticles synthesized through the aqueous route, Opt. Mater. **64**, 179–186 (2017).
9. B. Chandrasekar, R. Chandramohan, R. Vijayalakshmi, S. Chandrasekaran, Preparation and characterization of Mn-doped ZnS nanoparticles, Int. Nano. Lett. **5**, 71–75 (2015).
10. A. Ashkarran, Absence of photocatalytic activity in the presence of the photoluminescence property of Mn–ZnS Nanoparticles prepared by a facile wet chemical method at room temperature, Mater. Sci. Semicond. Process. **17**, 1–6 (2014).
11. Choi, S. Yoon, F. Sunjoo Kim, N. Kim, Aqueous-phase synthesis and color-tuning of core/shell/shell inorganic nanocrystals consisting of ZnSe, (Cu, Mn)-doped ZnS, and ZnS, J. Alloys Compd. **671**, 360-365 (2016).
12. Begum, A. Chattopadhyay, Redox-tuned three-color emission in double (Mn and Cu) doped zinc sulfide quantum dots, J. Phys. Chem. Lett. **5 (1)**, 126–130 (2014).
13. Sotelo-Gonzalez, L. Roces, S. Garcia-Granda, M.T. Fernandez-Arguelles, J.M. Costa-Fernandez, A. Sanz-Medel, Influence of Mn^{2+} concentration on Mn^{2+}-doped ZnS quantum dot synthesis: evaluation of the structural and photoluminescent properties, Nanoscale **5 (19)**, 9156–9161 (2013).
14. Pejjai, V.R.M. Reddy, K. Seku, T.R.R. Kotte, C. Park, Chemical bath deposition of Mn-doped ZnS thin films using greener complexing agents: effect of Mn-doping on the optical properties, Optik **130**, 608–618 (2017).
15. Kaur, M. Sharma, O.P. Pandey, Photoluminescence and photocatalytic studies of metal ions (Mn and Ni) doped ZnS nanoparticles, Opt. Mater. **47**, 7–17 (2015).
16. Viswanath, H.S. Bhojya Naika, G.S. Yashavanth Kumar, P.N. Prashanth Kumar, K.N. Harisha, M.C. Prabhakara, R. Praveen, Synthesis and photoluminescence enhancement of PVA capped Mn^{2+} doped

ZnS nanoparticles and observation of tunable dual emission: a new approach, Appl. Surf. Sci. **301**, 126-133 (2014).

17. V. Zaware, R.Y. Borse, B.G. Wagh, Properties of thin ZnS: Mn films sprayed by improved method: the role of Mn^{2+} ion concentration, Mater. Sci-Poland. **35**, 291–302 (2017).
18. Wang, P. Wang, B. Huang, X. Ma, G. Wang, Y. Dai, X. Zhang, X. Qin, Synthesis of Mn-doped ZnS microspheres with enhanced visible light photocatalytic activity, Appl. Surf. Sci. **391**, 557-564 (2017).
19. A. Reddy, G. Murali, B. Poornaprakash, R.P. Vijayalakshmi, B.K. Reddy, Structural, optical and magnetic properties of $Zn_{0.97-x}Cu_xCr_{0.03}S$ nanoparticles, Appl. Surf. Sci. **258**, 5206– 5211 (2012).
20. Wang, M. Yang, Y. Ren, J Fan, Cu-Mn codoped ZnS quantum dots-based ratiometric fluorescent sensor for folic acid, Anal. Chim. Acta **1040,** 136-142 (2018).
21. Ebrahimi, B. Yarmand, N. Naderi, Enhanced optoelectrical properties of Mn doped ZnS films deposited by spray pyrolysis for ultraviolet detection applications, Thin Solid Films **676,** 31–41 (2019).
22. Li, K. Liu, X. Zhu, M. Meng, W. Qin, Q. Liu, C. Xu, Competitive mechanism of electron transition in Mn-doped ZnS nanoribbons, J. Alloys Compd. **658**, 616-620 (2016).
23. S. Sabri, A.K. Yahya, M.K. Talari, Emission properties of Mn doped ZnO nanoparticles prepared by mechanochemical processing, J. Lumin. **132**, 1735–1739 (2012).
24. N. Bhargava, D. Gallaghar, X. Hong, A. Nurmikko, Optical properties of manganese-doped nanocrystals of ZnS, Phys. Rev. Lett. **72,** 416–419 (1994).
25. Zhu, S. Mei, W. Yang, G. Zhang, Q. Chen, W. Zhang, R. Guo, Tunable emission of Cu (Mn)-doped ZnInS quantum dots via dopant interaction, J. Colloid Interface Sci. **506**, 27–35 (2017).
26. Theyvaraju, S. Muthukumaran, Preparation, structural, photoluminescence and magnetic studies of Cu doped ZnO nanoparticles co-doped with Ni by sol-gel method, Physica E **74,** 93-100 (2015).
27. K. Ghosh, S.F. Ahmed, S. Jana, K.K. Chattopadhyay, Photoluminescence and field emission properties of ZnS:Mn nanoparticles synthesized by rf-magnetron sputtering technique, Opt. Mater. **29**, 1584–1590 (2007).
28. Mote, Y. Purushotham, B. Dole, Structural, morphological and optical properties of Mn doped ZnS nanocrystals, Cerâmica **59**, 614–619 (2013).
29. Yang, X. Zhao, X. Shan, H. Fan, L. Yang, Y. Zhang, Blue-shift of UV emission in ZnO/graphene composites, J. Alloys Compd. **556**, 1–5 (2013).
30. T. Tan, B.J. Chen, X.W. Sun, W.J. Fan, H.S. Kwok, X.H. Zhang, S.J. Chua, Blueshift of optical band gap in ZnO thin films grown by metal-organic chemical-vapor deposition, J. Appl. Phys. **98**, 013505 (2005).
31. S. Yoon, K.S. Lee, T.S. Lee, B. Cheong, D.K. Choi, D.H. Kim, W.M. Kim, Properties of fluorine doped ZnO thin films deposited by magnetron sputtering, Sol. Energy Mater. Sol. Cells **92,** 1366–1372 (2008).

32. Takagahara, K. Takeda, Theory of the quantum confinement effect on excitons in quantum dots of indirect-gap materials, Phys. Rev. B **46**, 15578 (1992).
33. Kuppayee, G.K. Vanathi Nachiyar, V. Ramasamy, Enhanced photoluminescence properties of ZnS:Cu^{2+} nanoparticles using PMMA and CTAB surfactants, Mat. Sci. Semicon. Proc. **15**, 136–144 (2012).
34. Nakamoto, Infrared and Raman Spectra of Inorganic and Coordination Compounds, 5 ed. John Wiley, New York, 1997.
35. B. Qadri, E.F. Skelton, D. Hsu, A.D. Dinsmore, J. Yang, H.F. Gray, B.R. Ratna, Size-induced transition-temperature reduction in nanoparticles of ZnS, Phys. Rev. B **60**, 9191 (1999).
36. S. Rema Devi, R. Raveendran, A.V. Vaidyan, Synthesis and characterization of Mn^{2+}-doped ZnS nanoparticles, Pramana—J. Phys. **68**, 679–687 (2007).
37. Tong, Z. Jiang, C. Wang, Z.Y. Xin, S. Hong, Liu, Effect of annealing on the morphology and properties of ZnS: Mn nanoparticles/PVP nanofibers, Mater. Lett. **62**, 3385-3387 (2008).
38. L. Faita, K. Ersching, C.M. Poffo, L.C. Benetti, D.M. Trichês, S.M. Souza, A.D.C. Viegas, J.C. de Lima, Structural, thermal, magnetic and optical characterization of undoped nanocrystalline ZnS prepared by solid state reaction, J. Alloys Compd. **590**, 176-183 (2014).
39. Bhattacharjee, Ch.-H. Lu, Multicolor luminescence of undoped zinc sulfide nanocrystalline thin films at room temperature, Thin Solid Films **514**, 132–137 (2006).
40. Hoheisel, V.L. Colvin, C.S. Johnson, A.P. Alivisatos, Threshold for quasicontinuum absorption and reduced luminescence efficiency in CdSe nanocrystals, J. Chem. Phys. **101**, 8455-8460 (1994).
41. Nasser, H. Elhouichet, M. Férid, Effect of Mn doping on structural, optical and photocatalytic behaviors of hydrothermal $Zn_{1-x}Mn_xS$ nanocrystals, Appl. Surf. Sci. **351**, 1122–1130 (2015).
42. Kar, S. Biswas, White light emission from surface-oxidized manganese-doped ZnS nanorods, J. Phys. Chem. C **112**, 11144–11149 (2008).
43. Pan, D. Yang, Y. Zhao, Z. Ma, G. Dong, J. Qiu, Facile hydrothermal synthesis of Mn doped ZnS nanocrystals and luminescence properties investigations, J. Alloys Compd. **579**, 300–304 (2013).
44. Xia, I.W. Lenggoro, K. Okuyama, Synthesis and photoluminescence of spherical ZnS:Mn^{2+} particles, Chem. Mater. **14**, 4969–4974 (2002).
45. Dong, L. Cao, G. Su, W. Liu, Synthesis and characterization of Mn doped ZnS d-dots with controllable dual-color emissions, J. Colloid Interface Sci. **367**, 178–182 (2012).
46. Datta, S. Biswas, S. Kar, S. Multicolor luminescence from transition metal ion (Mn^{2+} and Cu^{2+}) doped ZnS nanoparticles, Nanosci. Nanotechnol. **10**, 3670–3676 (2007).
47. Kole, C. Tiwary, P. Kumbhakar, Room temperature synthesis of Mn^{2+} doped ZnS d-dots and observation of tunable dual emission: effects of doping concentration, temperature, and ultraviolet light illumination, J. Appl. Phys. **113**, 114308 (2013).
48. Karar, F. Singh, B. Mehta, Structure and photoluminescence studies on ZnS: Mn nanoparticles, J. Appl. Phys. **95**, 656–660 (2004).

Figures

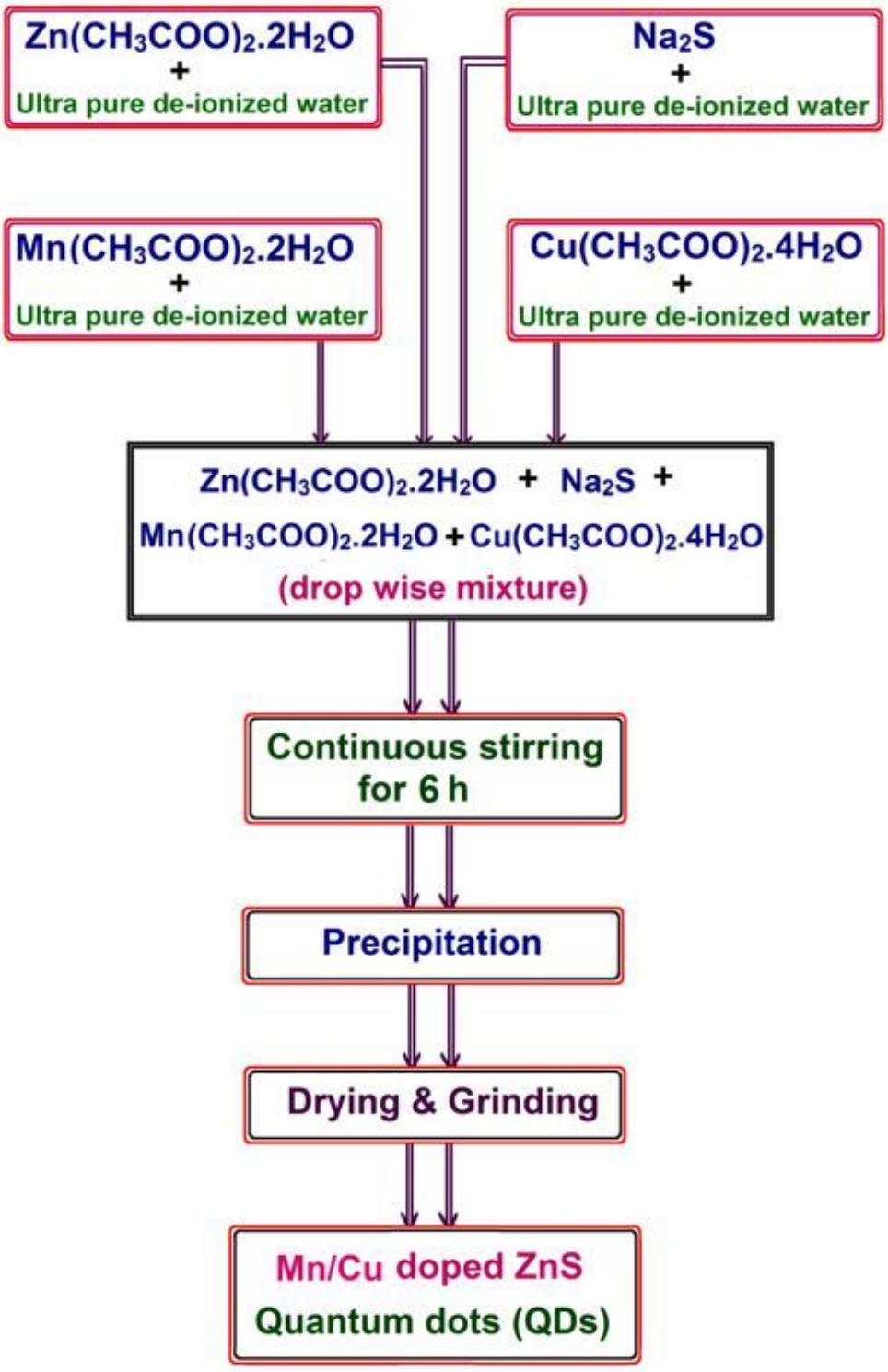

Figure 1

Flow chart for the preparation of Mn/Cu doped ZnS nanostructures.

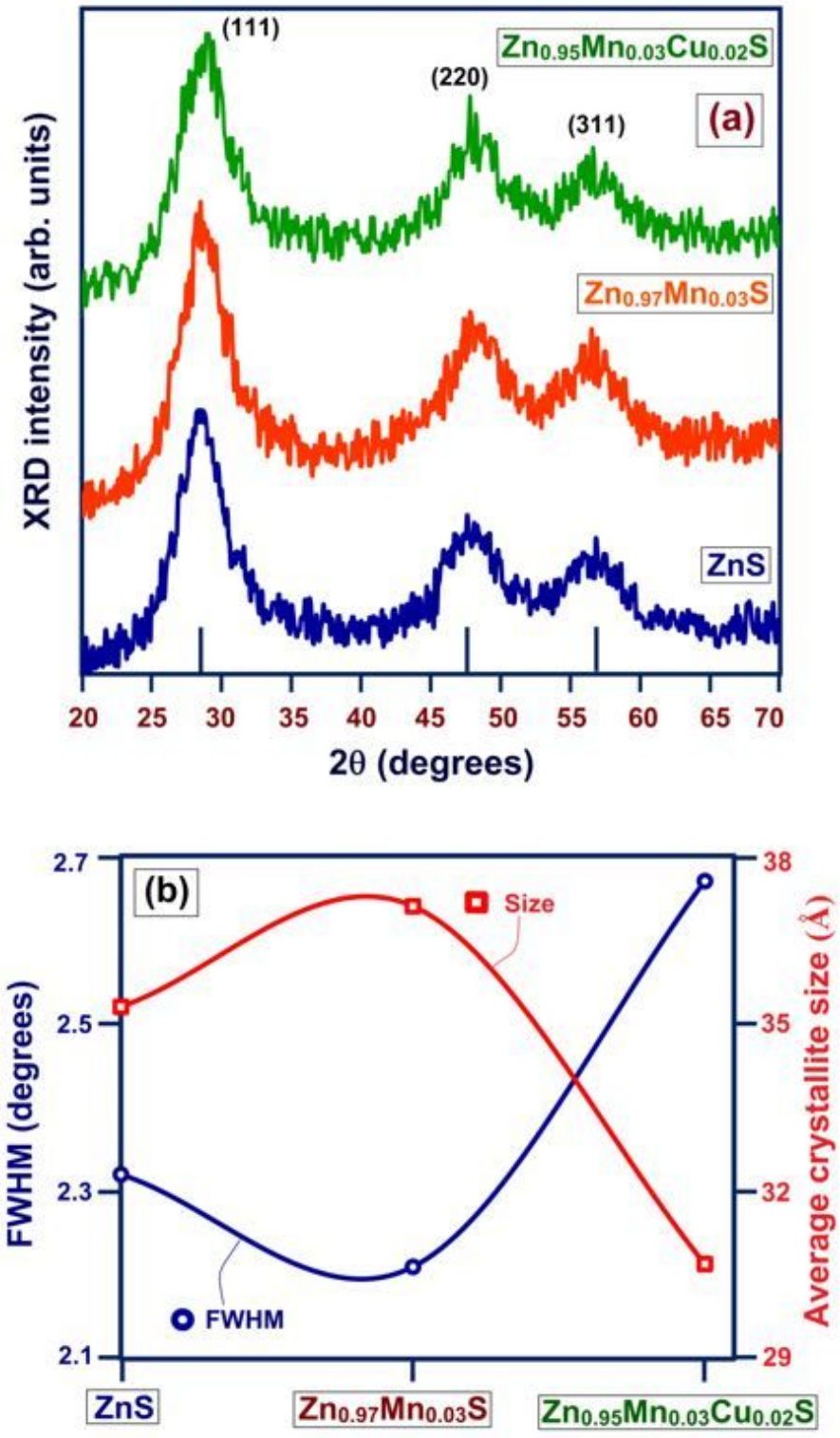

Figure 2

(a) The XRD pattern and (b) the variation of FWHM and average crystallite size of pure ZnS, Zn0.97Mn0.03S and Zn0.95Mn0.03Cu0.02S nanostructures

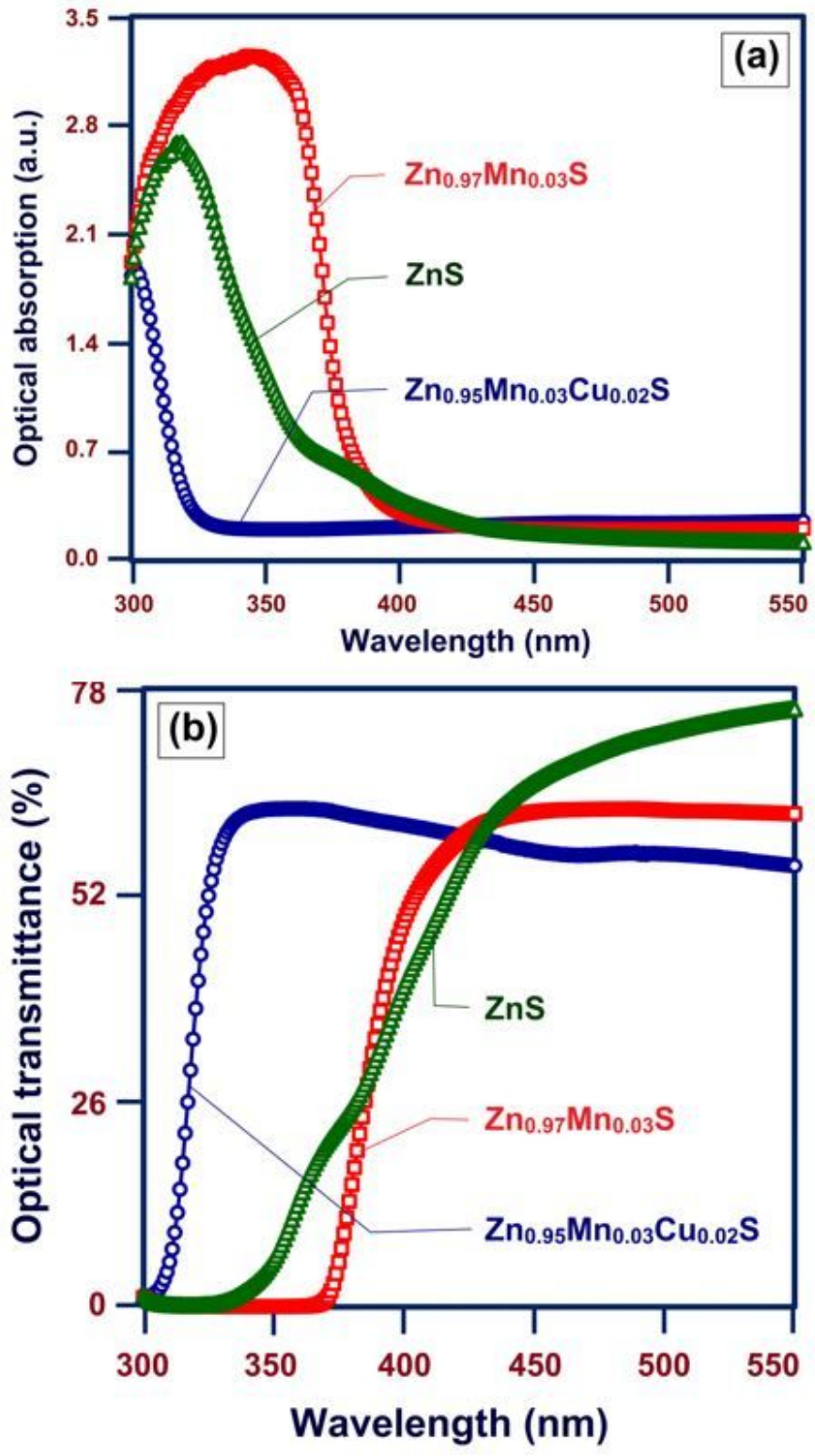

Figure 3

UV-visible (a) absorption spectra and (b) transmittance spectra of pure ZnS, Zn0.97Mn0.03S and Zn0.95Mn0.03Cu0.02S nanostructures from 300 nm to 550 nm.

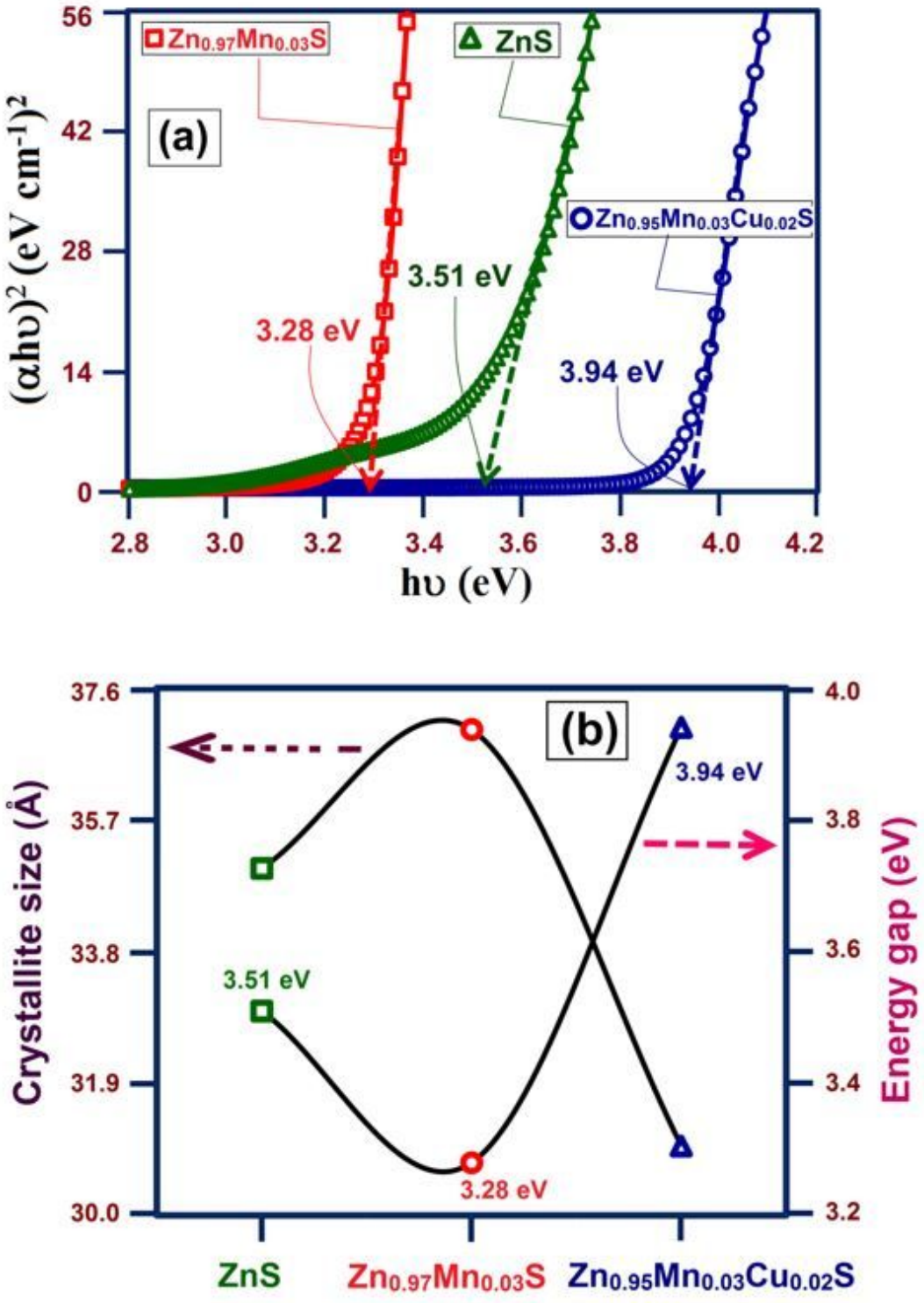

Figure 4

(a) The (αhυ)2 versus hυ curves for the optical band gap determination, (b) the modulation of crystallite size and energy gap of pure ZnS, Zn0.97Mn0.03S and Zn0.95Mn0.03Cu0.02S nanostructures.

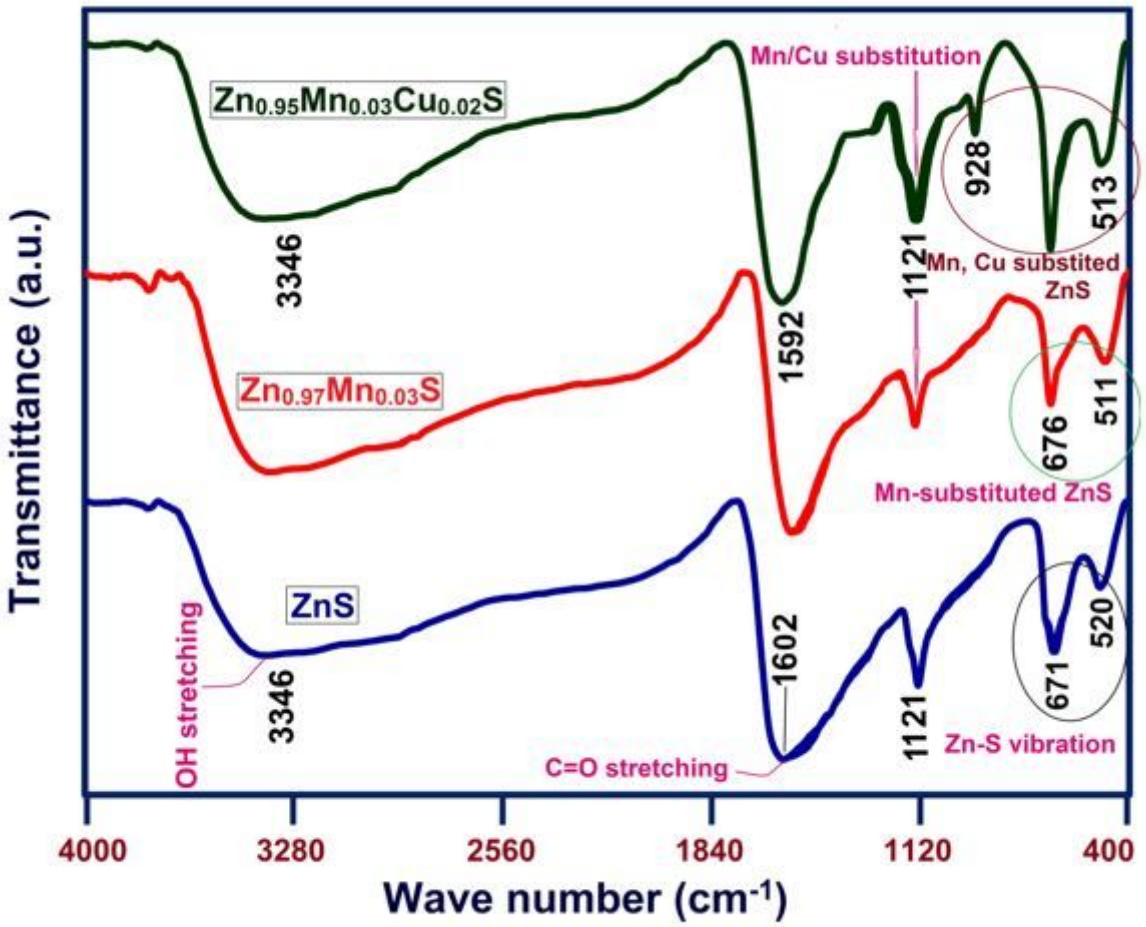

Figure 5

FTIR spectra of pure ZnS, Zn0.97Mn0.03S and Zn0.95Mn0.03Cu0.02S nanostructures in the wave number range from 400 to 4000 cm-1 at room temperature.

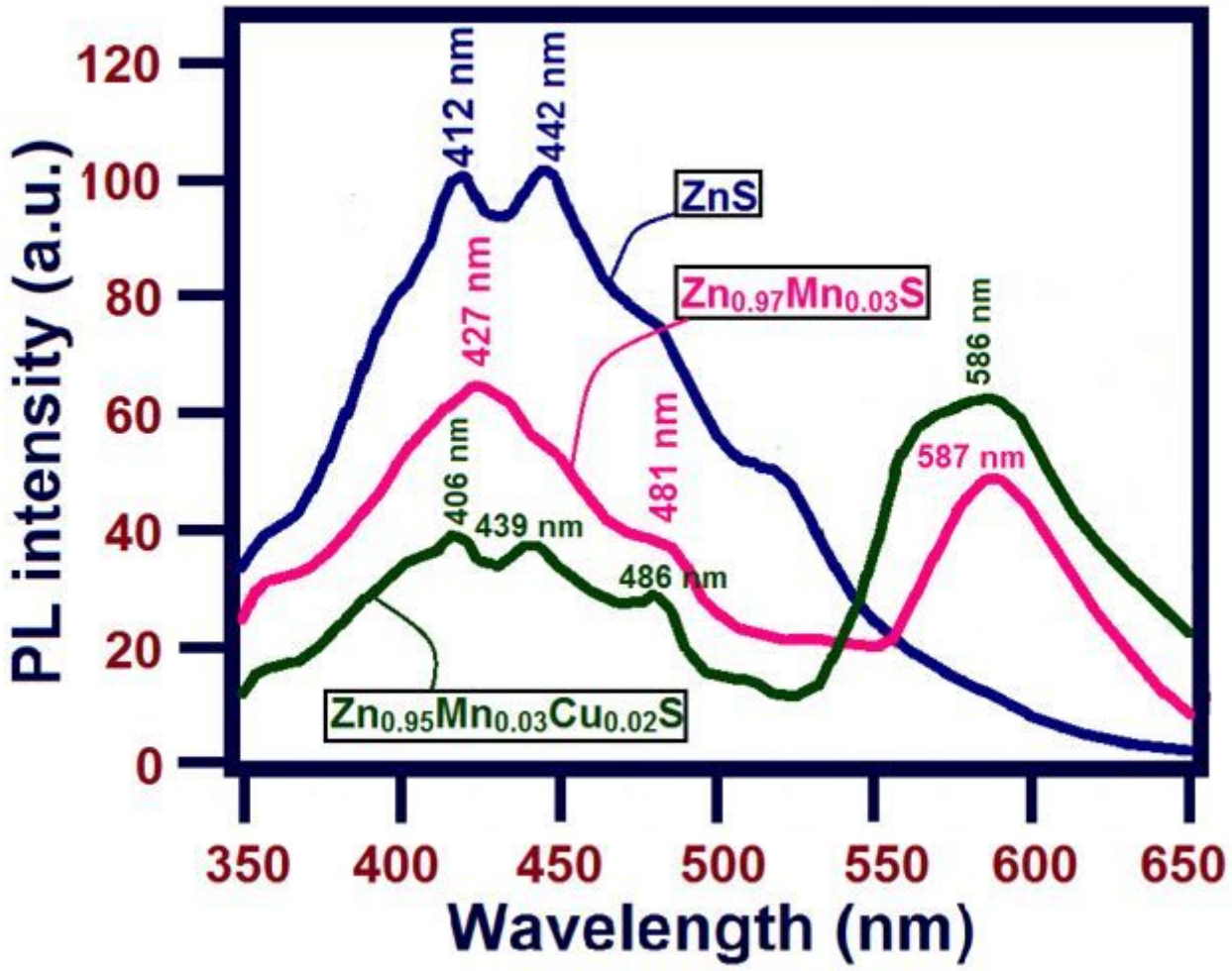

Figure 6

Room temperature photoluminescence spectra of pure ZnS, Zn0.97Mn0.03S and Zn0.95Mn0.03Cu0.02S nanostructures from 350 nm to 650 nm using 330 nm line of Xe excitation source.

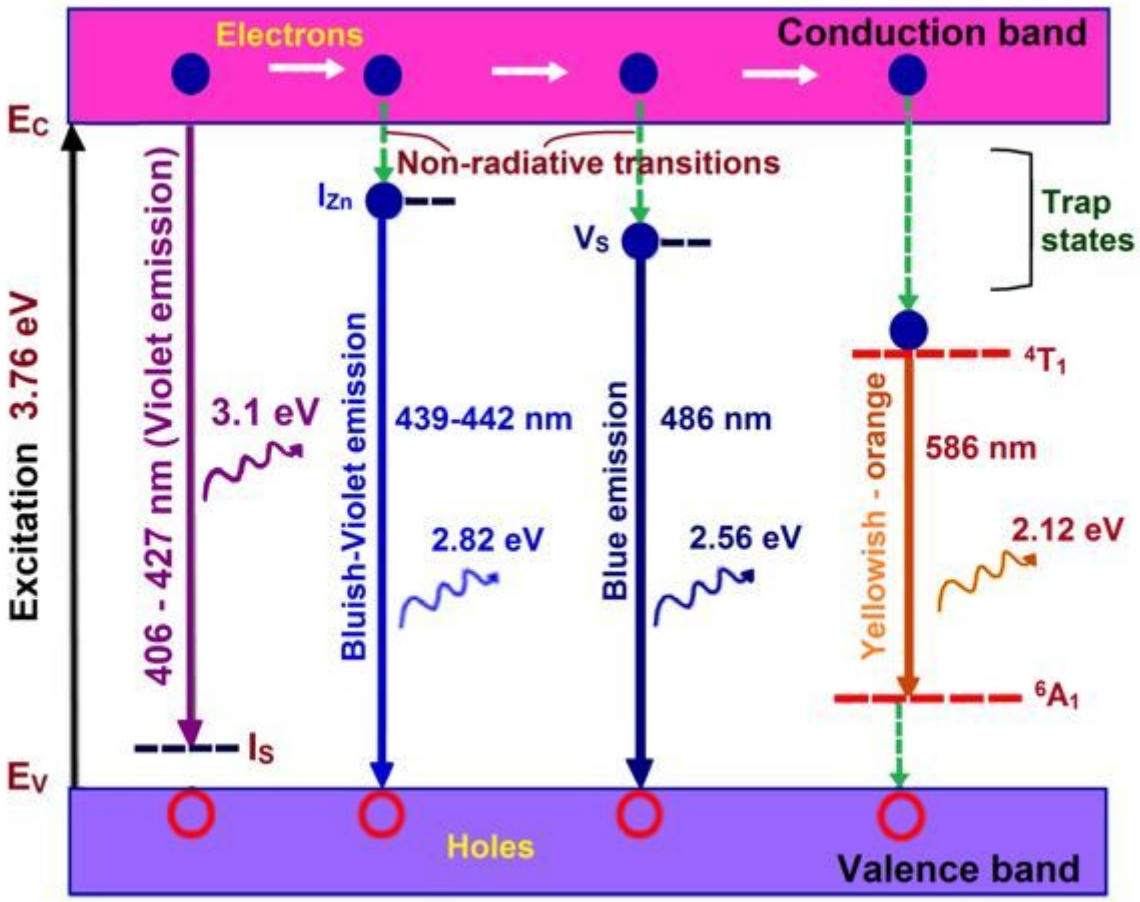

Figure 7

The energy level diagram of pure ZnS, Zn0.97Mn0.03S and Zn0.95Mn0.03Cu0.02S nanostructures to explain the various PL emissions like violet, blue and yellowish orange